Development of in silico models to guide the experimental characterisation of penile tissue and inform surgical treatment of erectile dysfunction

Fereidoonnezhad, B.; Akbarzadeh Khorshidi, M.; Bose, S.; Watschke, B.; Mareena, E.; Nolan, D.; Cooney, S.; Lally, C.

DOI
10.1016/j.compbiomed.2023.107524

Publication date
2023

Document Version
Final published version

Published in
Computers in Biology and Medicine

Computers in Biology and Medicine 166 (2023) 107524

Contents lists available at ScienceDirect

Computers in Biology and Medicine

journal homepage: www.elsevier.com/locate/compbiomed

Development of *in silico* models to guide the experimental characterisation of penile tissue and inform surgical treatment of erectile dysfunction

B. Fereidoonnezhad [a,1], M. Akbarzadeh Khorshidi [b,c,d,1], S. Bose [b,c,d], B. Watschke [e], E. Mareena [f], D. Nolan [f], S. Cooney [f], C. Lally [b,c,d,*]

[a] Department of Biomechanical Engineering, Delft University of Technology, Delft, 2628CD, the Netherlands
[b] Trinity Centre for Biomedical Engineering, Trinity Biomedical Sciences Institute, Trinity College Dublin, Dublin, Ireland
[c] Department of Mechanical, Manufacturing & Biomedical Engineering, School of Engineering, Trinity College Dublin, Ireland
[d] Advanced Materials and Bioengineering Research Centre (AMBER), Royal College of Surgeons in Ireland and Trinity College Dublin, Dublin, Ireland
[e] Urology, Boston Scientific Corp, Inc, Minnetonka, MN, USA
[f] Urology, Boston Scientific Corp, Inc, Clonmel, Co. Tipperary, Ireland

ARTICLE INFO

Keywords:
Penile tissue
Indentation testing
Compression testing
Hyperelastic model
FEA
Mechanical characteristics
IPP implantation

ABSTRACT

This paper presents a computational study to investigate the mechanical properties of human penile tissues. Different experimental testing regimes, namely indentation and plate-compression tests, are compared to establish the most suitable testing regime for establishing the mechanical properties of the different penile tissues. An idealised MRI-based geometry of the penis, containing different tissue layers, is simulated using the finite element (FE) method to enable realistic predictions of the deformation of the penis. Unlike the linear elastic models used in the literature to-date, hyperelastic isotropic/anisotropic material models are used to capture material nonlinearity and anisotropy. The influence of material properties, morphological variations, material nonlinearity and anisotropy are investigated. Moreover, the implantation of an inflatable penile prosthesis (IPP) is simulated to assess the effects of the implantation procedure, material nonlinearity, and anisotropy on tissue stresses. The results indicate that the interior layers of the penis do not affect the overall stiffness of the penis in the indentation test, while the plate-compression test is able to capture the effects of these layers. Tunica Albuginea (TA) is found to have the most significant contribution to the total stiffness of the penis under load. It can also be observed that buckling occurs in the septum of the penis during the compression tests, and different morphologies dictate different compressive behaviours. There is a clear need for future experimental studies on penile tissues given the lack of relevant test data in the literature. Based on this study, plate-compression testing would offer the most insightful experimental data for such tissue characterisation.

1. Introduction

Erectile dysfunction (ED) is an increasing male health concern estimated to affect approximately 322 million men worldwide by 2025 [1]. Currently, ED is reported to affect 52% of the male population within the age group of 40–70 [2], and its prevalence increases by about 10% for each decade of life after 50 years [3]. Despite being so common, ED still remains an undiagnosed and undertreated disease in many men, leading to an inferior quality of life [4].

There are several treatment methods for ED including oral pharmacotherapy, topical/intraurethral alprostadil, low-intensity shock-wave therapy, vacuum erection devices, and intracavernous injection [5]. However, many ED sufferers (e.g., those suffering from diabetes or vascular diseases) do not respond well to these therapies and are advised to use penile implants [6]. Several types of penile implants are commercially available such as malleable penile prostheses (MPPs), and 2- or 3-piece inflatable penile prostheses (IPPs). Penile implants consist of a pair of cylinders which are placed in the corpus cavernosa (CC) of the penis and can be inflatable (for IPPs) or non-inflatable (for MPPs). IPPs also have a pump (in scrotal sacs) which enables the transportation of fluid to the cylinders to increase pressure within them. In the 3-piece IPP, a reservoir placed in the lower abdomen stores the fluid. Over 25,

* Corresponding author. Trinity College Dublin, Dublin 2, Ireland.
E-mail address: lallyca@tcd.ie (C. Lally).
[1] Joint first author – both authors equally contributed to this study.

https://doi.org/10.1016/j.compbiomed.2023.107524
Received 17 July 2023; Received in revised form 24 August 2023; Accepted 19 September 2023
Available online 26 September 2023

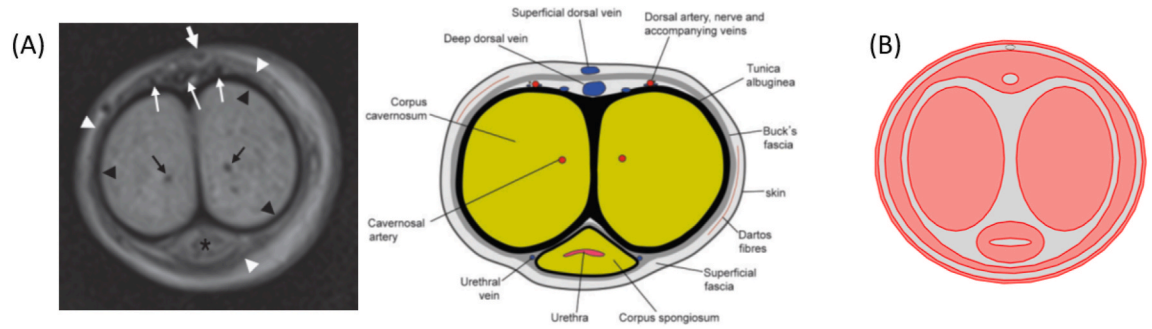

Fig. 1. (A) MRI scan and schematic of penis cross section [27], (B) the FE model constructed from the MRI scan.

000 IPPs are implanted in the US annually [7].

Although IPPs have been effective in dealing with ED, long-term usage can cause tissue damage (e.g. fibrosis) and device malpositioning [8] due to the inflation/deflation of the cylinders. In addition, IPPs can pose a risk of infection, bleeding/hematoma and there is also a risk of mechanical failure of the device [8]. The mechanical survival rate of the IPPs varies from 57 to 76% after 15 years of implantation [9]. The limited durability of IPPs is linked to fibrosis, tissue erosion and mechanical durability which are all governed by the mechanical behaviour of penile tissue and its interaction with the implant.

In silico modelling is a powerful tool for preclinical assessment of medical devices and surgical treatment planning, and could therefore offer the potential to improve outcomes for ED treatment. Such *in silico* models can provide fundamental insights into the poor clinical outcomes following IPP implantation in some patients, and can also be used to optimise or even personalise device design and treatment procedures. Well characterised mechanical properties of penile tissues and anatomically accurate geometries of the penis are, however, key factors for the development of reliable *in silico* models.

To-date, some studies have been conducted to develop FE models of penile tissue and IPP implantation. Early studies on modelling the penis showed the structural rigidity of the organ and the role of tunica albuginea (TA) in load-bearing [10–12]. Gefen et al. [13] developed 2D penile models which were used to assess the interaction between the IPP cylinder and the penile tissue during erection and the levels of internal stress generated in diabetic and non-diabetic patients [14]. Mohamed et al. [15] showed the importance of a two-chambered penile structure that possesses greater stability during erection. Another set of 3D computational models analysed the stress distributions in an asymmetric penis and patients with Peyronie's disease [16]. Tissue properties obtained from experiments conducted using indenters were used to develop the model [17]. A study by Levy et al. [18] on a wide variety of penile compression clamps (PPCs), demonstrated the importance of a minor misalignment of the PCCs, leading to stress concentrations and high tissue strains which could be associated with discomfort and pain. These models have several limitations that reduces their usability for the accurate prediction of clinical outcomes and device design optimisation. The major limitation of these models is that the penile tissues have been considered to be linear-elastic materials with somewhat arbitrary material properties, that are not based on empirical data. Moreover, an idealised anatomical geometry of the penis has been used in most of the available FE models.

The lack of tissue properties used to develop the models is attributed to the very limited reporting of penile tissue testing. A study by Timm et al. [17] developed an indentation test for *in vivo* characterisation of the mechanical properties of human penile tissue. However, this technique created local deformation in the tissues and was therefore relatively insensitive to the mechanical properties of the internal layers such as TA, CC, and corpus spongiosum (CS). Although some studies estimated the stiffness (100 MPa) and tensile strength (0.001–0.01 MPa) of TA using tensiometers, they did not report the strain generated in the tissue [19]. A recent study by Brady et al. [20], characterised the tissue properties of TA specimens with varying levels of calcification (0–28% volume ratio). A very wide variation in tissue stiffness (11.8–55.3 MPa) was observed due to the irregular specimen geometry, varying levels of calcification and irregular mineralization patterns. A few studies have reported the stiffness of CC (18.5–25.2 kPa) using shear wave elastography (SWE), however, the full non-linear stress-strain behaviour cannot be extracted from such techniques to inform the computational models as SWE assumes linear elasticity [21–23]. To date, one study has reported the stiffness of penile foreskin (2.85–3.01 MPa) [24], whilst there is no mechanical data available for the penile fascial layers, to the authors' knowledge.

The lack of knowledge on the biomechanical properties of penile tissues provides a significant obstacle to the development of pre-clinical testbeds for next-generation IPPs with improved outcomes [25]. Cadaveric studies provide some insight into the mechanical properties; however, such tissues are often fixed with formaldehyde resulting in a stiffer tissue response as compared to fresh tissue [26]. Animal penile tissue isalso not a good representative of the human tissue, as human penis is significantly different from both smaller animals (e.g., rats and rabbits) and larger animals (e.g., horses and dogs) in terms of anatomy. Therefore, a non-destructive methodology is required for *in vivo* mechanical characterisation of human penis tissue layers.

This paper presents finite element simulations to study the mechanical responses of different layers of the penile tissue (such as TA, CC and CS). A suitable mechanical test method where the overall mechanical response of the tissue is sensitive to the mechanical properties of the internal layers of the penis is required for this investigation. In the first part of this study, we show that *in-vivo* indentation test results, proposed in Ref. [17], are not sensitive to the mechanical properties of the internal penile tissue components (such as TA, CC and CS). Therefore, this technique is not suitable for characterisation of the mechanical properties of internal layers. We then propose a plate compression test as an alternative method for the *in vivo* mechanical characterisation of penile tissue, where the results of the plate compression test demonstrate that it is more sensitive to the mechanical properties of CC, CS and TA layers, compared to the indentation test. Using these FE simulations, we also investigate the influence of material models and penile geometry on the results of the plate compression test. Finally, we simulate the IPP implantation procedure and compare the tissue response for different device implantation scenarios.

2. Materials and methods

The sensitivity of the mechanical response of the intact penis to the mechanical properties and shape/size of different penile tissue components (i.e., TA, CC, and CS) are investigated using finite element (FE) simulations in Abaqus 2022 (Simulia). The details of the FE models are presented in the following sections.

Table 1
Mechanical properties of penile tissue components. TA = tunica albuginea, CC = corpus cavernosum, CS = corpus spongiosum, BF=Buck's fascia, SF = superficial fascia, S = skin, U = urethra, B = blood.

	TA	CC	CS	BF	SF	S	U	B
μ (MPa)	4.2857	0.0071	0.0071	25	25	0.1786	0.0071	0.0001
κ (MPa)	20	0.0333	0.0333	116.96	116.96	0.8333	0.0333	0.005
Ref.	[14]	[14]	[14]	[27]	[27]	[14]	–	–

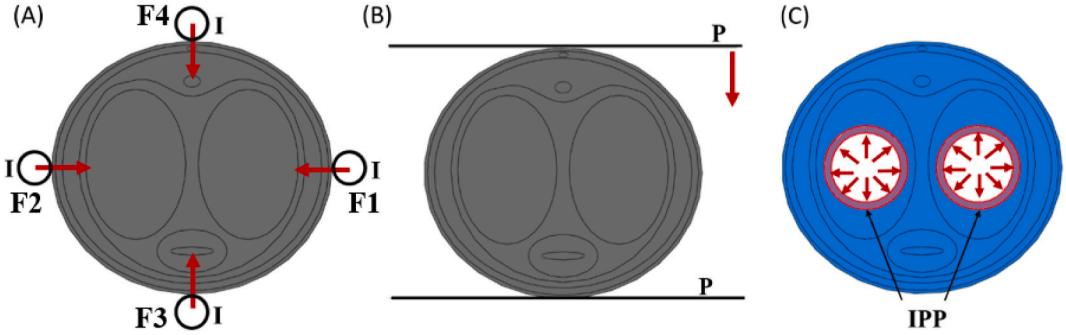

Fig. 2. Finite element model of (A) Indenter test, (B) Plate compression test, and (C) IPP implantation.

2.1. FE model of penis

The geometry of a penis cross-section is reconstructed from a magnetic resonance image (MRI) [27], as shown in Fig. 1. The reconstructed model is composed of skin, Buck's fascia, superficial fascia, tunica albuginea (TA), corpus cavernosum (CC), corpus spongiosum (CS), urethra, superficial dorsal vein, and deep dorsal vein. Due to the absence of anatomical data in the axial direction, a 2D plane strain model is created. Subsequently, a 3D model is recontructed by extruding the 2D sketch.

Initially, a neo-Hookean (NH) isotropic hyperelastic model is used to represent the mechanical behaviour of all tissue components. This model is represented by the strain energy density function ψ as [28]:

$$\psi = \frac{\mu}{2}(\bar{I}_1 - 3) + \frac{\kappa}{2}(J-1)^2 \tag{1}$$

where, μ is the initial shear modulus, κ is the initial bulk modulus, $J = \det(\mathbf{F})$ is the volume ratio, and $\bar{I}_1 = \text{trace}(\overline{\mathbf{C}})$ is the first strain invariant. $\mathbf{F}$ here represents the deformation gradient tensor and $\overline{\mathbf{C}} = \overline{\mathbf{F}}^{\mathrm{T}}\overline{\mathbf{F}}$ is the right Cauchy-Green tensor in which $\overline{\mathbf{F}} = (J^{-1/3})\mathbf{F}$. The values of μ and κ are calculated based on the reported values of Young's modulus and Poisson's ratio in the literature as presented in Table 1.

$$\mu = \frac{E}{2(1+\nu)}, \kappa = \frac{E}{3(1-2\nu)} \tag{2}$$

Blood is modelled as a neo-Hookean material with a very low shear modulus and high bulk modulus to represent an incompressible fluid. Moreover, for the sake of simplicity, we ignore the role of the thin urethra in the mechanical response of the tissue. The same material properties as the CS are assigned to the urethra. The Poisson's ratio of all tissues (except blood) is assumed to be 0.4 [14], implying their representation as compressible materials. A Poisson's ratio approaching 0.5 results in infinite bulk modulus, signifying incompressiblity. In our case, we assume compressibility given that the Poisson's ratio is less than 0.45. The Poisson's ratio of blood is assumed equal to 0.49 to enforce incompressibility.

2.2. Testing approaches

2.2.1. Compression test simulation

2.2.1.1. Material properties. In order to study the effects of tissue characteristics, an appropriate testing approach is required. To this end, the only non-destructive full penile organ testing presented in the literature is examined. This test technique, proposed by Timm et al. [17], uses four indenters to impose force at four separate quadrants (F1, F2, F3 and F4) of the tissue as shown in Fig. 2a. The indenters apply local pressure to the tissue. Given this localised nature of the loading, an alternative testing approach, namely a plate-compression test, was also employed to establish if this alternative test method would provide additional insights into the mechanical behaviour of the individual tissue components. In this approach, two rigid plates impose a compressive load on the tissue as shown in Fig. 2b. In the next section, we show a comparison between the indentation and compression tests using the FE simulations. The realistic geometry of the penis' cross section obtained from MRI (Fig. 1a) is used to generate the 2D FE model. The results of this comparison are discussed in section 3.1. In this study, we investigate the influence of morphology, material nonlinearity, material anisotropy, and implantation procedure on the mechanical response of the penile tissue.

2.2.1.2. Morphological variations. To illustrate the effect of morphology, four different penile cross-sectional geometries are considered. The first geometry corresponds to the idealised geometry obtained from MRI, called the *baseline*. In all subsequent cases, all the parameters are constant except CC and CS are scaled up by a factor of 1.07 and 1.12, respectively. To study the effects of morphological variations, we compare the results of the baseline geometry with geometries with bigger CC, bigger CS and non-symmetric CC.

In addition, three different thicknesses of TA are compared to the baseline. The outer boundary of TA is adjusted using scale factors of 0.98, 1.02, and 1.05 relative to the baseline. It is important to note that the boundaries of the remaining layers remain unchanged; specifically, only the Buck's fascia layer becomes thinner as the TA thickness increases.

2.2.1.3. Material nonlinearity. To study the effect of material nonlinearity, the Ogden hyperelastic model is utilised. This constitutive model is

Table 2
Material parameters of the Ogden hyperelastic model for tunica albuginea obtained from the experimental data in Ref. [20] and the values of Young's modulus and Poisson's ratio reported in Ref. [14].

μ_1 (MPa)	α_1	μ_2 (MPa)	α_2	D_1 (MPa^{-1})	D_2 (MPa^{-1})
0.8	8.0	0.8	−8.0	0.001	0.001
2.14285	8.0	2.14285	−8.0	0.1	0.1

Table 3
Material parameters of neo-Hookean hyperelastic model for tunica albuginea obtained from the experimental data [20].

μ (MPa)	κ (MPa)
1.6	2000

able to capture a higher level of nonlinearity in the stress-strain behaviour when compared to the neo-Hookean model. The strain energy density function of the Ogden model is [26].

$$\psi = \sum_{i=1}^{N} \frac{2\mu_i}{\alpha_i^2}\left(\bar{\lambda}_1^{\alpha_i} + \bar{\lambda}_2^{\alpha_i} + \bar{\lambda}_3^{\alpha_i} - 3\right) + \sum_{i=1}^{N} \frac{1}{D_i}(J-1)^{2i} \tag{3}$$

where $\bar{\lambda}_i = J^{-1/3}\lambda_i$ $(i = 1, 2, 3)$ are the distortional principal stretches, $D_i = 2/\kappa_i$ and α_i are material parameters. The initial shear and bulk moduli for the Ogden form are given by

$$\mu_0 = \sum_{i=1}^{N} \mu_i, \kappa_0 = \frac{2}{D_1} \tag{4}$$

In this study, two separate sets of material properties have been used for TA, from Brady et al. [20] and Gefen et al. [14]. First, the ogden hyperelastic model is adopted to match the experimental data from tensile tests on TA from the work by Brady et al. [20]. It is noted the TA used in Ref. [20] was obtained from participants suffering from Peyronie's disease. We considered the specimen with minimum fibrotic and calcified portion as representative of healthy tissue. The calibrated parameters of the Ogden model are presented in Table 2. The corresponding small strain Young's modulus and Poisson's ratio are calculated from the parameters in Table 2, using the relationship between Lamé's constants. Then, the material parameters of the neo-Hookean hyperelastic model are calculated using these Young's modulus and Poisson's ratio as shown in Table 3. Second, material parameters (μ_1, μ_2, D_1 and D_2) of the Ogden hyperelastic model for TA (Table 2) are obtained from the reported values of Young's modulus and Poisson's ratio by Gefen et al. [14] corresponding to the neo-Hookean parameters introduced in Table 1 ($\mu_1 = \mu_2 = \mu/2$ and $D_1 = D_2 = D$). Here, a second-order Ogden model with the same nonlinearity level ($\alpha_1 = -\alpha_2 = 8$) is employed for a better comparison with the parameters calibrated from Brady et al. [20]. Thereafter, the FE simulations are carried out using the Ogden hyperelastic and neo-Hookean hyperelastic models under the plate compression test and the remaining tissue layers are defined using Table 1.

2.2.1.4. Material anisotropy. Previous studies available in the literature indicate that the TA has different stiffness in different directions due to fibre orientations within this layer [30–33]. To capture the role of material anisotropy, TA is assumed to be a fibrous material that can be defined using the Holzapfel-Gasser-Ogden (HGO) anisotropic hyperelastic model. The strain energy density function for the HGO model in Abaqus is defined by the following function [34,35].

$$\psi = C_{10}(\bar{I}_1 - 3) + \frac{k_1}{2k_2}\sum_{i=1}^{N}\left[e^{k_2\langle\bar{E}_i\rangle^2} - 1\right] + \frac{1}{D}\left(\frac{J^2-1}{2} - ln\, J\right) \tag{5}$$

where C_{10} and k_1 are stress-like material parameters which denote the initial (isotropic) stiffness and fibre stiffness, respectively, and k_2 is a dimensionless material parameter representing the nonlinear contribution of fibres to the total strain energy, D is a material parameter which has an inverse relationship with the bulk modulus to represent material compressibility ($D > 0$ represents the compressible tissue while $D = 0$ denotes the incompressibility condition), and N denotes the number of families of fibres within the material. Also, $\bar{E} = d(\bar{I}_1 - 3) + (1 - 3d)(\bar{I}_4 - 1)$ in which d expresses the level of dispersion in the fibre directions ($d = 0$ means that the fibres are perfectly aligned and there is no dispersion in them, the maximum value for this parameter is 1/3 which means fibres are randomly oriented and it acts as an isotropic material), and $\bar{I}_4 = \bar{\mathbf{C}} : (\boldsymbol{a}_i \otimes \boldsymbol{a}_i)$ is an invariant of the right Cauchy-Green tensor $\bar{\mathbf{C}} = \bar{\mathbf{F}}^t\bar{\mathbf{F}}$ and $\mathbf{A}_i = \boldsymbol{a}_i \otimes \boldsymbol{a}_i$ in which $\boldsymbol{a}_i$ are direction vectors of each corresponding family of fibres. Note that N in Eq. (4) is the number of fibre families and $\langle x\rangle = (x + |x|)/2$ is the ramp function.

Since C_{10} represents the stiffness of the matrix material, the same shear modulus for TA presented in Table 1 is used to define this parameter, $C_{10} = \mu/2 = 2.14285$ MPa, and the compressibility parameter is defined using the bulk modulus of TA presented in Table 1 as $D = 2/\kappa = 0.1$ MPa^{-1}. We also use a neo-Hookean model with the parameters of Table 1 for other layers. To assess the influences of k_1 and k_2 on the total compressive stiffness of the whole tissue, a 2D finite element model is employed. In this case, the fibre orientation is assumed circumferential in TA where the fibres follow the elliptical shape of CC as shown in Fig. 7 and the dispersion of fibres is assumed fully aligned, $d = 0$. To assess the effects of fibre orientation and dispersion on the compression test response, a 3D finite element model is created to describe the out-of-plane fibre directions. The same cross-section shown in Fig. 1b is extruded to form a 30 mm 3D geometry of the penis. In this 3D simulation, TA is defined by the HGO model with $C_{10} = \mu/2 = 2.14285$ MPa, $D = 2/\kappa = 0.1$ MPa^{-1}, $k_1 = 10$ and $k_2 = 10$, and the rest of the layers are defined by a neo-Hookean model with parameters shown in Table 1. Three cases have been outlined for the fibre angle, α, in TA; $\alpha = 0^\circ$ (longitudinal direction of fibres), $\alpha = 90^\circ$ (circumferential direction of fibres), and $\alpha = 45^\circ$ (helical direction of fibres).

Table 4
Material parameters of Ogden hyperelastic model for corpus cavernosum (CC) estimated based on the shear modulus presented by Gefen et al. [14].

μ_1 (MPa)	α_1	μ_2 (MPa)	α_2	D_1 (MPa^{-1})	D_2 (MPa^{-1})
0.00355	8.0	0.00355	−8.0	60.06	60.06

2.2.2. FE simulation of IPP implantation

2.2.2.1. IPP implantation procedure. In addition, an IPP implantation is simulated based on the MRI-based geometry and neo-Hookean hyperelastic models with the properties shown in Table 1. In this simulation, two cylinders are implanted into CC (see Fig. 2c) and expanded to simulate the erectile conditions. IPP deployment in CC is performed for two different clinically relevant scenarios: (i) Corpus cavernosum tissue is removed so that the cylinders fit into the cavity after tissue removal (Scenario I), and (ii) no tissue is removed, and the cylinders are pushed into the tissue and then inflated (Scenario II). To simulate Scenario I, two holes of diameter 12 mm are made in the CC chambers and two cylinders of outer diameter 12 mm are implanted in the holes. A radial displacement of 1.5 mm is applied to the outer surface of the cylinders. In implantation without tissue removal (Scenario II), a dilator is used to dilate the corpora in order to facilitate the insertion of cylinders into CC. Therefore, to simulate scenario II, smaller holes with diameters 6 mm are created in the CC chambers and two cylinders of outer diameters 6 mm are implanted in these holes. The radial displacement for this scenario is 4.5 mm, therefore, the initial diameter of the holes in scenario II is half that of Scenario I, yet the final diameters after IPP expansion are

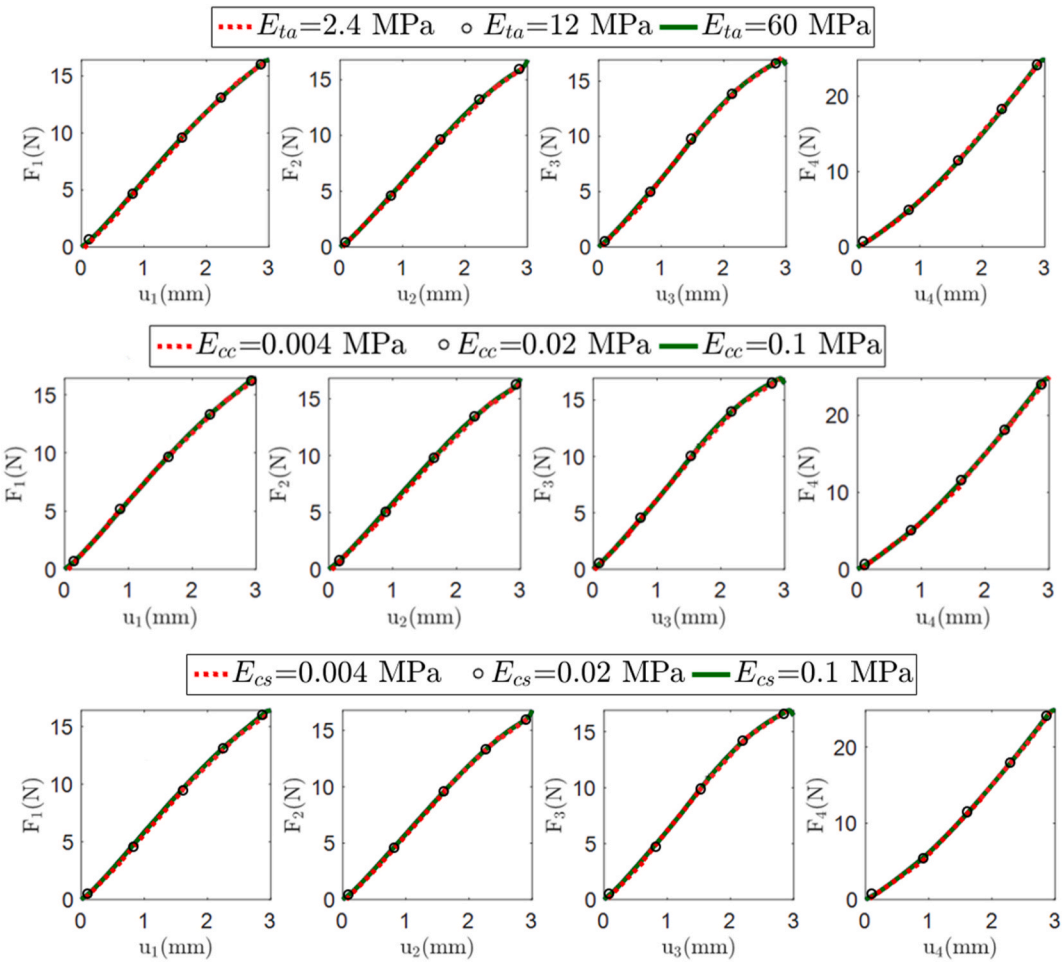

Fig. 3. Influence of the mechanical properties of Tunica Albuginea (TA) (first row), Corpus Cavernosum (CC) (second row), and Corpus Spongiosum (CS) (third row) on the overall response of the penis in the indentation test.

the same for both.

2.2.2.2. Material nonlinearity. A second-order Ogden hyperelastic model is employed to investigate the effect of material nonlinearity on the IPP expansion simulations. Three cases are considered: (i) Ogden model is used for CC and neo-Hookean model for all other layers (case 1); (ii) Ogden model is applied to TA (based on Table 4 where the initial shear modulus is based on the results presented by Gefen et al. [14]) while neo-Hookean model is used for all other layers (case 2); (iii) Ogden model is applied to TA (based on Table 2 where the parameters are extracted from the experiments performed by Brady et al. [20]) and neo-Hookean model is used for all other layers (case 3). The Ogden model parameters used for CC are shown in Table 4 (for case 1). In this table, μ_1, μ_2 and D_1 are estimated using Eq. (3), D_2 is assumed the same as D_1, and $\alpha_1 = -\alpha_2 = 8$ is used to consider a similar level of nonlinearity compared to TA.

2.2.2.3. Material anisotropy. Similar to section 2.2.1.4, the HGO anisotropic hyperelastic model is employed to describe the effect of material anisotropy on IPP expansion. This model is applied to TA ($C_{10} = \mu/2 = 2.14285$ MPa and $D = 2/\kappa = 0.1$ MPa^{-1}) and other layers are defined using the neo-Hookean model (Table 1). For the sake of simplicity, only the first scenario of IPP implantation is used in this section. Also, only point 3 (at the middle of TA septum) is considered for

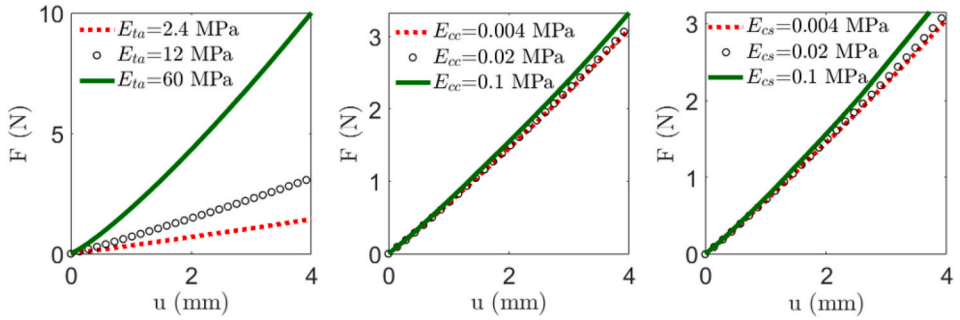

Fig. 4. Influence of the mechanical properties of Tunica Albuginea (TA), Corpus Cavernosum (CC), and Corpus Spongiosum (CS) on the overall response of the penis in the plate compression test.

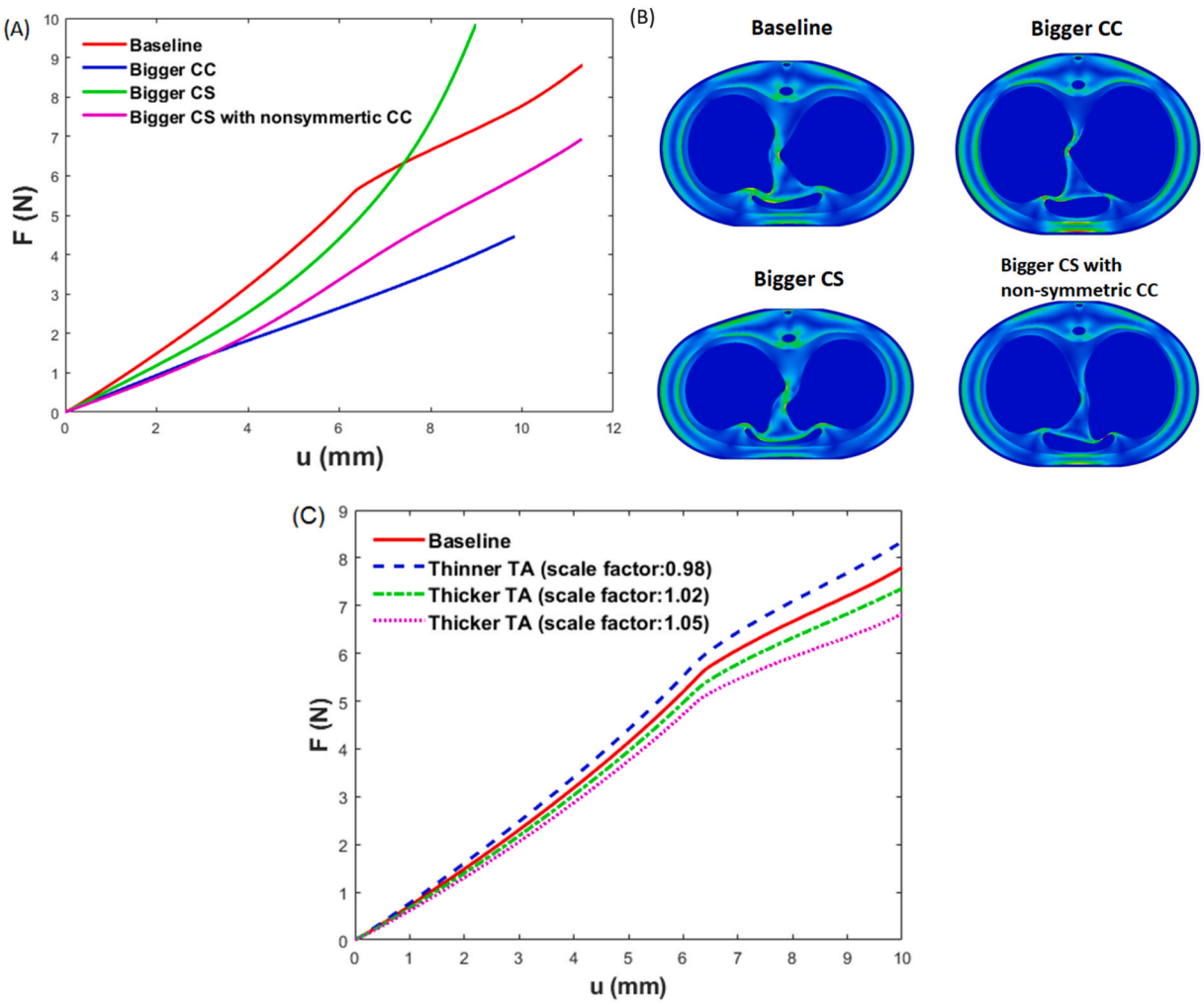

Fig. 5. Influence of morphological variations of the penis on its overall mechanical response in the compression test; (A) the force-displacement responses of four cases, (B) the compression mechanisms for each case, and (C) the force-displacement responses for different TA thicknesses.

the results analysis.

A mesh study is performed to determine the required mesh density for a converged solution; 5284 quadrilateral elements for 2D compression/indentation tests, 7856 quadrilateral elements for 2D IPP-expansion simulation (Scenario I), 14,599 quadrilateral elements for 2D IPP-expansion (Scenario II), 338,160 hexahedral elements for 3D compression test, and 949,275 hexahedral elements for 3D IPP-expansion simulation, are found to be sufficient for convergence of the results and minimum change in the reaction force for the compression test and von Mises stress for IPP inflation (<1%).

3. Results and discussions

3.1. Compression test simulation

3.1.1. Role of mechanical properties

The results show that the force-displacement curves for each actuator in the indentation test are not sensitive to variations in stiffness of the different layers (i.e. TA, CC, and CS), in the investigated range of displacements. This is illustrated in Fig. 3. The reason for such a response is that the indentation test induces only local deformations under the indenters rather than a bulk deformation of the whole tissue. In contrast, the plate compression test shows sensitivity to changes in tissue properties because it induces deformation in the whole tissue domain and the overall response of the whole organ is influenced by the stiffness of each layer. The results obtained from the plate compression testing also indicate that TA stiffness dominates the force response of the organ. Fig. 4 demonstrates the plate compression test results.

3.1.2. Role of morphological variations

The results indicate that the morphological variations have a considerable impact on the total stiffness of the tissue, as shown in Fig. 5. The baseline penis geometry experiences a weakening at $u = 6.3$ mm where the TA septum buckles followed by a decrease in the total stiffness of the penis. The bigger CC model requires less force than the baseline model due to the reduced thickness of TA (TA is much stiffer than CC) with a thinner septum as the size of CC increases. Therefore, the buckling of the septum occurs sooner ($<u = 3$ mm) and the tissue fails at a lower displacement. Although the tissue's stiffness in *Bigger CS* is less than *Baseline* due to the thinner TA, the buckling surprisingly happens at a higher displacement ($u = 9$ mm). This is due to the fact that the septum has more space (bigger CS) to move under the applied load until it experiences the compressive load to buckle (see supplementary files). In this case, there is a higher compressive strength after the buckling of the septum. Asymmetry in the geometry with non-symmetric CC causes early buckling of the TA septum between the left and right CC. Following this, a mixture of septum bending and CS compression is observed which allows the tissue to have a better resistance during the compression, that is, bending of the septum doesn't occur quickly because the energy applied is simultaneously consumed to bend the septum and compress

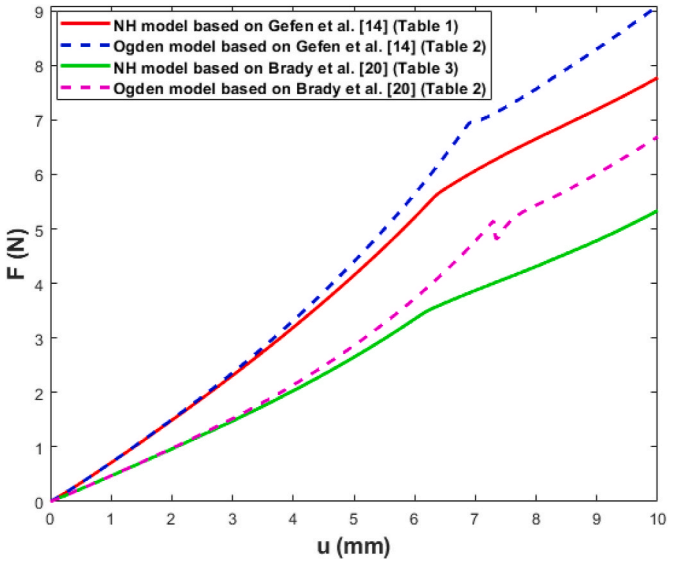

Fig. 6. Influence of material nonlinearity of Tunica Albuginea (TA) on the overall response of penile tissue in compression testing.

the CS. When the CS is fully compressed ($u = 7.5$ mm), the septum bends more easily, resulting in the observed drop in the stiffness of the tissue.

In Fig. 5C, we analyse the impact of TA thickness, observing that a thicker TA—resulting in a thinner fascia layer—correlates with reduced stiffness in the tissue during the plate-compression test. It is important to note that this altered thickness does not affect the point of tissue weakening (buckling), thus confirming that the septum governs buckling. Note that the TA septum thickness remains identical to the baseline across these three scenarios.

3.1.3. *Role of material nonlinearity*

The results reveal the significant role of material nonlinearity on the overall mechanical response of the penis, highlighting the importance of layer-specific mechanical characterisation of penile tissue, as illustrated in Fig. 6. This figure shows that changing the material nonlinearity can change the compressive behaviour of the tissue where the increase in the stiffness is followed by a weakening response due to septum buckling. In fact, the level of nonlinearity in the Ogden hyperelastic model is higher than the neo-Hookean hyperelastic model, therefore, the former is able to sustain a higher level of nonlinear stresses during the compression. This can affect both the total tissue stiffness and septum buckling. It is observed from Fig. 6 that both hyperelastic models have the same response in smaller displacements (u < 4 mm), while for larger displacements, the results are considerably different.

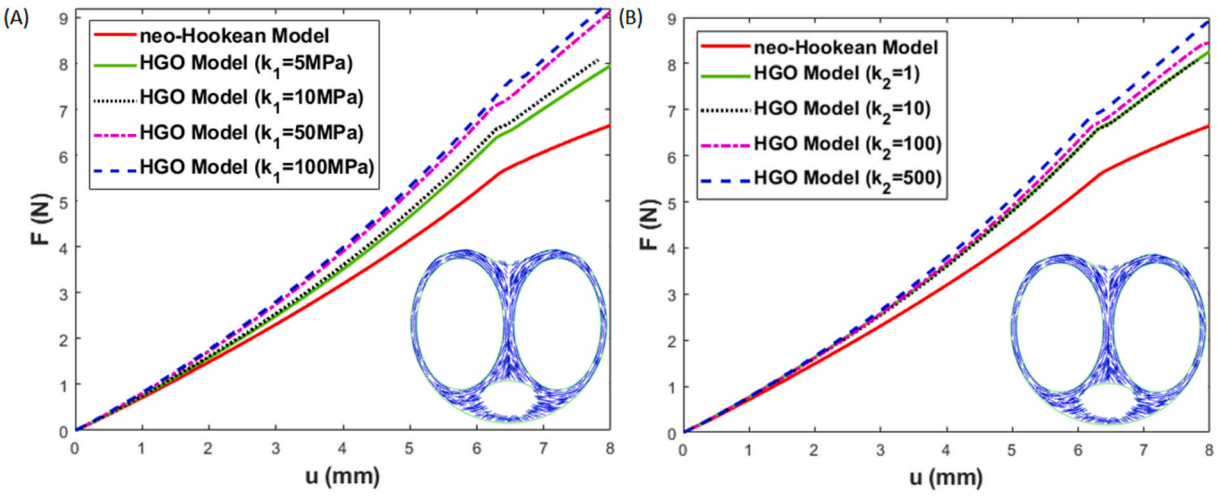

Fig. 7. Influence of parameters (A) k_1 ($k_2 = 10$) and (B) k_2 ($k_1 = 10$ MPa) used in TA on the overall response of penile tissue in compression test.

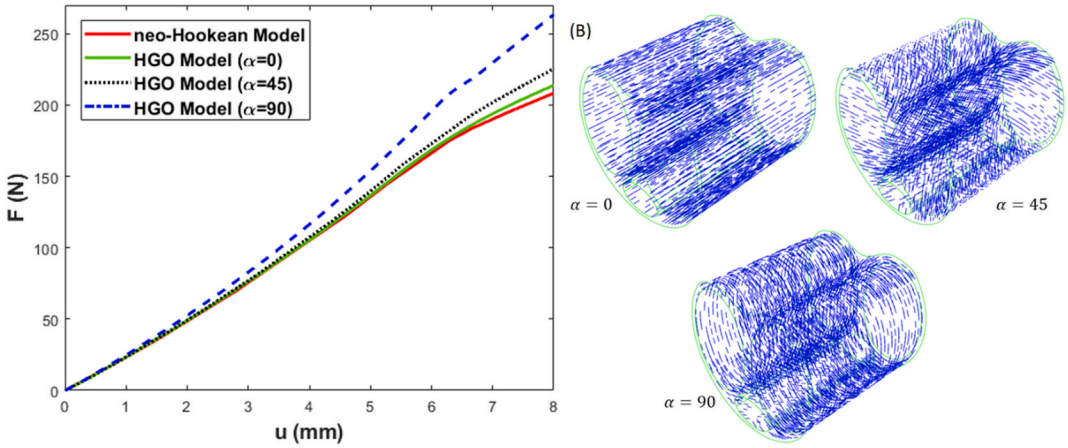

Fig. 8. (A) Influence of fibre orientation in TA on the overall response of penile tissue in compression testing (d = 0). (B) Different fibre orientations in TA.

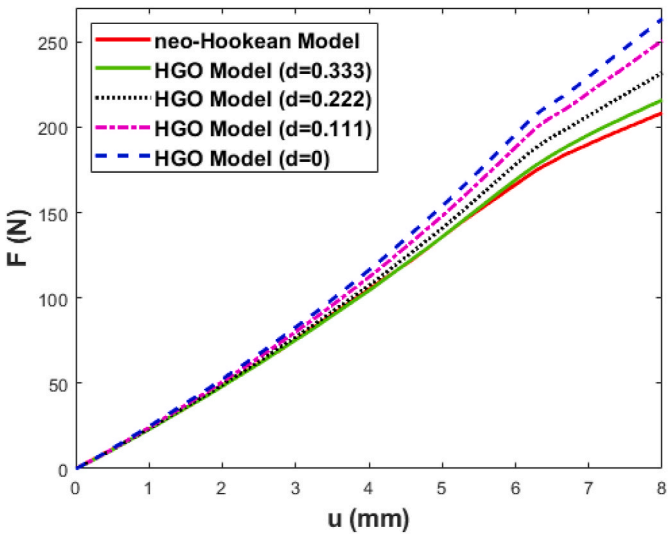

Fig. 9. Influence of fibre dispersion in TA on the overall response of penile tissue in compression testing (α = 90).

3.1.4. Role of material anisotropy

The influence of k_1 and k_2 on the total compressive stiffness of the tissue is illustrated in Fig. 7a and b, respectively, where the HGO model predicts a stiffer tissue than the neo-Hookean model. At high displacements, the stiffness of the tissue increases as k_1 increases. Although changing k_2 has an impact on the overall compressive response, as compared to Neo-Hookean, increasing this parameter does not markedly change the overall tissue response.

Fig. 8a shows the effects of fibre orientation on the 3D compression test. As can be observed, the circumferentially oriented fibres in TA cause the most dramatic stiffness increase in the compressive response of the penile tissue. In contrast, the longitudinal fibres orientation has a negligible impact. In fact, fibres do not contribute to the compressive stiffness of the tissue in $\alpha = 0$. The influence of fibre dispersion is depicted in Fig. 9. Note that $d = 0$ means that fibres align perfectly in the circumferential direction, and $d = 0.333$ refers to an isotropic material and in this case leads to the same results as the longitudinal fibre orientation.

3.2. FE simulation of IPP implantation

3.2.1. IPP implantation procedure

The results of an IPP implantation simulation for the two deployment scenarios are shown here. As shown in Fig. 10, three points in the tissue (two points in CC and one point in TA) are considered for results analysis; point 1: the inner side of CC between the cylinder and the septum where the maximum stress in CC occurs (Inn_CC), point 2: the outer layer of CC between the cylinder and the septum (Out_CC), and point 3: the middle of the septum in TA (Mid_TA) where the maximum stress/strain in TA can be observed. The von Mises stress in the two scenarios of IPP implantation/expansion are compared in Fig. 11. The results indicate that the tissue generally undergoes a higher stress in the second implantation scenario, as more expansion is needed in this scenario. The biggest difference between these two scenarios can be measured in point 1 and the smallest difference occurs at point 3.

3.2.2. Role of material nonlinearity

The von Mises stress difference percentages between scenarios I and II for all three points mentioned in section 3.2.1 and all cases defined in section 2.2.2.2 are compared in Table 5. The stress differences are calculated for the maximum expansion ($D = 15$ mm). More remarkable differences are found between the first and second scenarios while using the Ogden model for CC (Case 1), as increasing the material nonlinearity allows CC to deform nonlinearly (with higher-level of nonlinearity). In addition, for Case 2 and Case 3 (the Ogden material models in TA) and while employing the neo-Hookean model for all layers, the greatest differences can be observed in the inner point of CC (point 1). It can be concluded that CC is more sensitive to material nonlinearity, and it is therefore crucial to define an appropriate material model for this layer to capture realistic material nonlinearity during IPP expansion.

The von Mises stresses obtained from the case in which all layers of penile tissue are neo-Hookean materials are compared to those obtained from Cases 1, 2 and 3 (including the Ogden hyperelastic model), as illustrated in Fig. 12. The figure reveals that material nonlinearity significantly affects the tissue stress level during IPP expansion. Due to the fact that CC plays an important role in IPP expansion, from an early stage of the expansion, Case 1 shows different stress levels compared with the CC neo-hookean model and the stress difference begins from the lower level of expansion ($D = 13.5$ mm). Although this deviation from the neo-Hookean model occurs later in cases 2 and 3 (respectively in $D = 14.25$ mm and $D = 14$ mm), these cases display a higher level of nonlinearity. The main observation concluded from Table 5 and Fig. 12 is that CC plays the most important role in IPP expansion. Note that only scenario I and point 3 (Mid-TA) are considered in this figure for the brevity of the results.

3.2.3. Role of material anisotropy

The influences of k_1 and k_2 on the IPP expansion simulation are illustrated in Fig. 13. The results indicate that the fibre stiffness (k_1) considerably influences the von Mises stress calculated in the TA septum (Fig. 13a) at higher levels of expansion (D > 14 mm). k_2 also appears to have a greater impact on material behaviour during IPP expansion simulation compared to the compression test, see Fig. 13b and Fig. 7b. This is due to the fact that the level of fibre stretch in expansion is higher than during the compression testing.

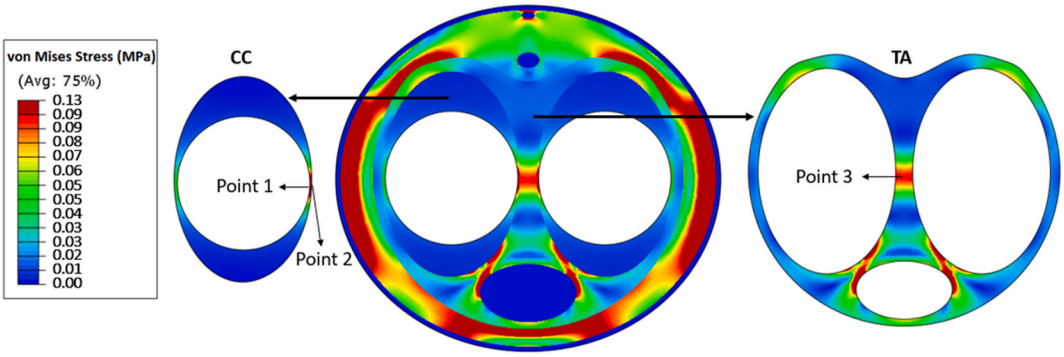

Fig. 10. Three points chosen to compare the results between the two scenarios (this plot shows the first scenario of implantation in which the cylinder's outer diameter is 13.8 mm).

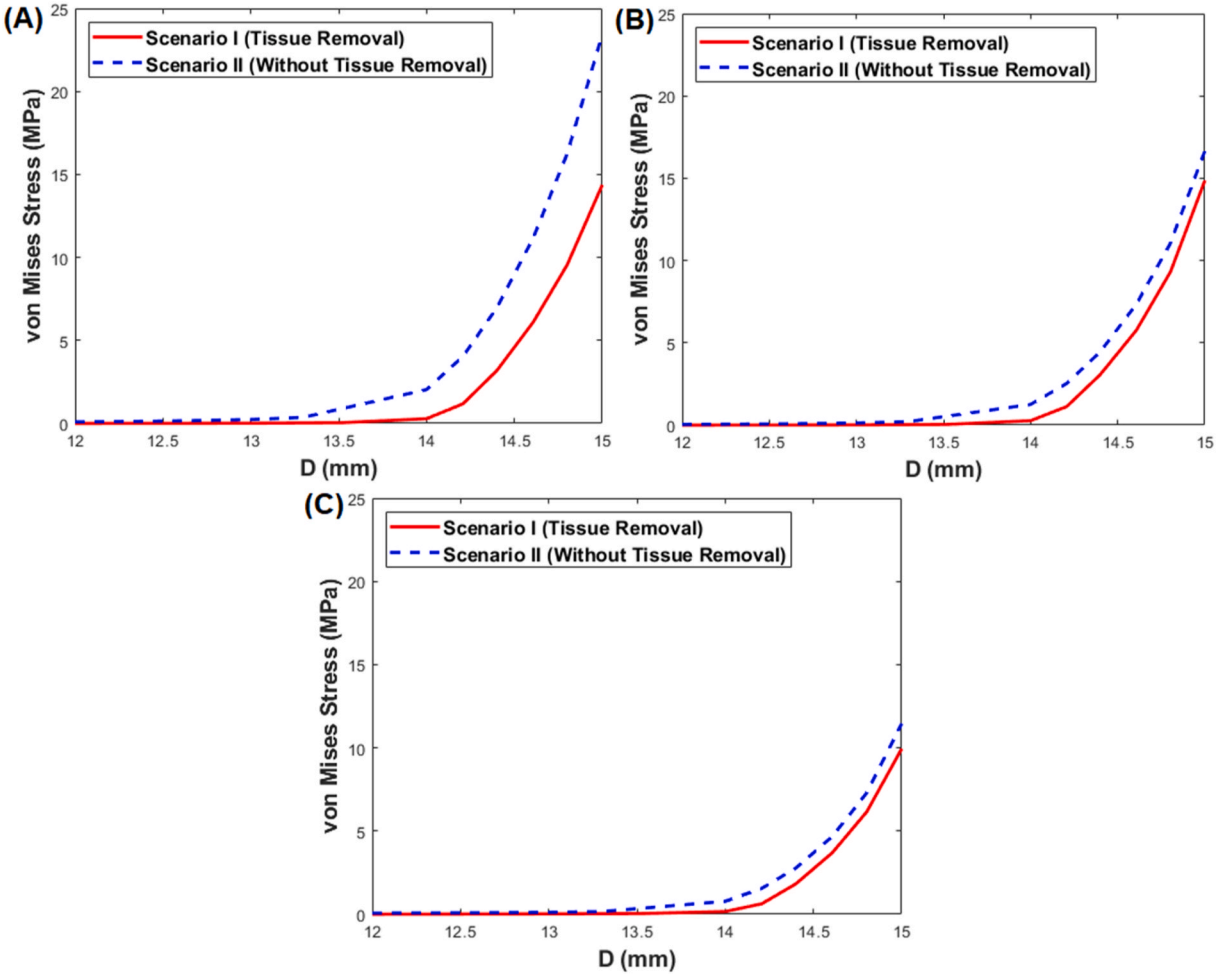

Fig. 11. Comparison of von-Mises stresses between two IPP implantation scenarios when neo-Hookean hyperelastic model is used for all tissue layers, (A) point 1 (Inn_CC), (B) point 2 (Out_CC), and (C) point 3 (Mid_TA).

Table 5
The percentage of the von Mises stress difference between scenarios I and II when the outer diameter IPP cylinder is D = 15 mm, von Mises stress difference (%) $= 100 \times \frac{S_{II} - S_I}{S_{II}}$ where S_I and S_{II} are von Mises stresses calculated for scenarios I and II, respectively.

	Point 1 (Inner_CC)	Point 2 (Outer_CC)	Point 3 (Mid_TA)
Case 1	96.46	96.42	97.12
Case 2	25.20	9.40	13.66
Case 3	50.97	10.82	9.23
neo-Hookean model (all layers)	39.16	11.51	14.05

When looking at fibre angles, similar to the compression test, $\alpha = 90$ produces the highest stress level in the septum, whereas $\alpha = 0$, longitudinal fibres, approximately reproduces the isotropic condition, see Fig. 14. Fibre dispersion in the 3D IPP expansion simulation, where the fibre direction is assumed to be circumferential ($\alpha = 90$), shows that the stress responses changes from an anisotropic ($d = 0$) state to the isotropic one ($d = 0.333$) as d increases, see Fig. 14b.

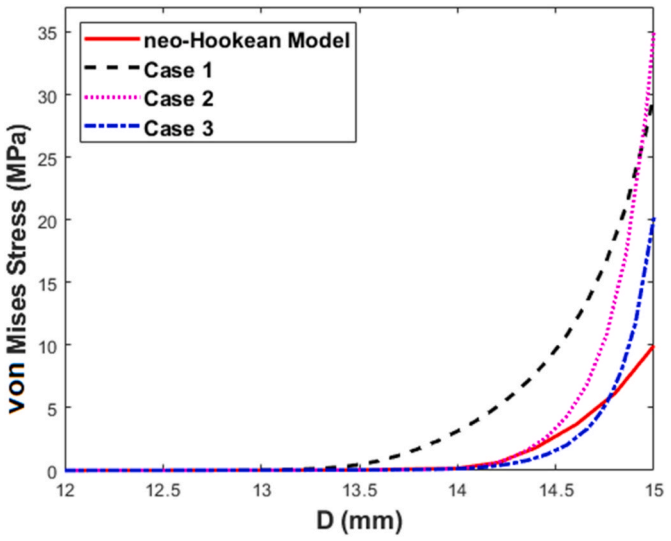

Fig. 12. Influence of material nonlinearity in the IPP expansion simulation (scenario I and point 3 (Mid_TA)).

4. Concluding remarks

This paper presents a finite element-based computational study to characterise the mechanical behaviour of penile tissue and evaluate testing regimes. The role of different parameters in the mechanical response of the tissue, and the interaction between the penile tissue and an inflatable penile prosthesis (IPP) have been investigated.

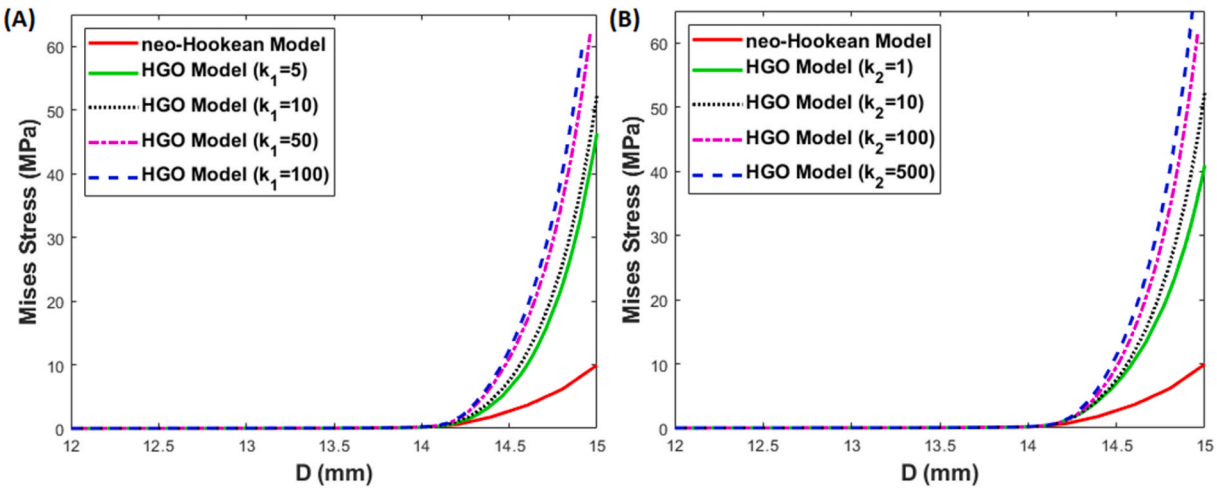

Fig. 13. Influence of parameters (A) k_1 ($k_2 = 10$) and (B) k_2 ($k_1 = 10$ MPa) used in Tunica Albuginea (TA) on the response of penile tissue in IPP expansion simulation ($\alpha = 90^\circ$ and $d = 0$).

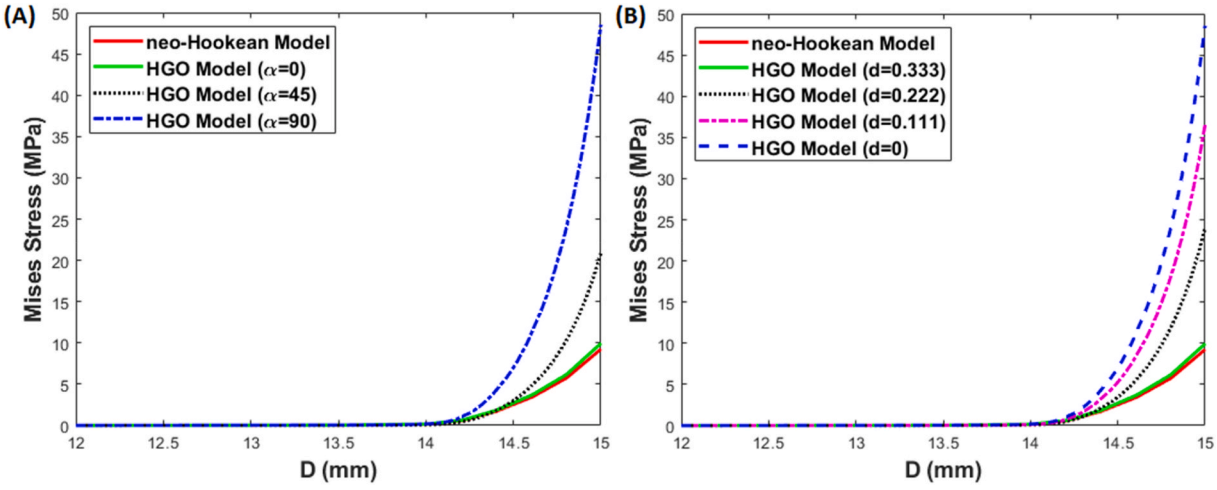

Fig. 14. Influence of (A) fibre orientation and (B) fibre dispersion (in $\alpha = 90$) in Tunica Albuginea (TA) on the response of penile tissue in IPP expansion simulation ($k_2 = 10$ and $k_1 = 10$ MPa).

Hyperelastic material models and an idealised MRI-based geometry have been employed to investigate the mechanical behaviour of penile tissue under both compression and expansion.

The results obtained reveal that an indentation test is not an appropriate non-destructive testing approach to examine the mechanical characteristics of penile tissue, and that plate-compression testing offers an alternative in which the effects of material properties of each layer are measurable. Therefore, this compression test has been employed, in this paper, to explore the roles of morphology, material properties, nonlinearity, and anisotropy in the compressive stiffness of the tissue. According to the results obtained from the compression test simulations, the shape and size of each layer play an essential role in the global stiffness of the tissue. Another key factor is the type of material model used for each layer. The hyperelastic material models are able to describe the more realistic mechanical response of the tissue, both material nonlinearity and anisotropy, when compared to the linear elastic model. Material nonlinearity influences both the compression and expansion behaviour of the tissue, while the role of material anisotropy is more significant in the IPP expansion simulation. Moreover, two scenarios of IPP implantation have been examined in this paper. These scenarios are based on the conventional procedures to implant IPP inside the penis, with and without tissue removal. The results indicate that implantation without tissue removal results in more tissue compression during the IPP expansion. As a result, higher stresses occur in the most affected layers, CC and TA. It can be concluded that using a highly nonlinear material model (e.g. the second-order Ogden hyperelastic model) in CC can strongly affect the response of whole tissue to IPP expansion. The finite element simulations of IPP implantation developed in this paper provide a predictive tool to assess the performance of the IPP implantation procedure. The results of this study lay the foundation for creating anatomically and biomechanically accurate *in silico* penile models. Such models hold the potential to serve as a platform for testing, optimising, and re-designing IPP procedures, with the aim of enhancing the overall efficacy and long-term success of these surgical interventions. Additionally, such models aid manufacturers and clinicians in minimising surgical difficulties, post-implantation complications and common tissue-device interactions such as fibrosis associated with IPP. However, the integration of a 3D penis scan to define the penile geometry would enhance the precision of the 3D model, thus potentially yielding simulation outcomes that more closely align with real-world expectations.

Future studies should concentrate on the mechanical characterisation of penile tissues due to the limitation in the testing data in the literature. The material models and some material parameters used in this study are hypothesised in order to predict the tissue responses, make comparisons, and elucidate the effect of different parameters. To better

understand the mechanics of the tissue, a comprehensive experimental study involving full organ testing and mechanical testing on individual layers is needed. As this study reveals, the mechanical properties of each layer, especially TA and CC, are vitally important in both the compression and expansion of penile tissue. Such experimental characterisation on TA and CC will be highly beneficial to develop a more realistic and robust penile model. In addition, the experimental plate-compression test or full-circular testing would provide the possibility of implementing an inverse finite element method (iFEM) to acquire the material parameters for individual layers (i.e. CC, CS, TA). The demonstrated importance of penis morphological variations on the mechanical response of the tissue also supports the need for *in vivo* imaging of ED sufferers to enable development of patient specific FE models and *in silico* models of virtual IPP implantations. Due to the absence of mechanical data from *in vivo* IPP performance, an extensive experimental study focusing on inflation/deflation of IPP devices into penile tissues will be vitally important. Then, the developed finite element simulation results can be compared and validated against such experiments.

Declaration of competing interest

The authors declare the following financial interests/personal relationships which may be considered as potential competing interests: Brian Watschke, E. Mareena, D. Nolan, S. Cooney are all employees of Boston Scientific Corporation.

Acknowledgement

The authors acknowledge the financial support of Science Foundation Ireland (SFI) under grant number 12/RC/2278_2 and Boston Scientific Limited (Clonmel).

Appendix A. Supplementary data

Supplementary data to this article can be found online at https://doi.org/10.1016/j.compbiomed.2023.107524.

References

[1] I.A. Ayta, J.B. McKinlay, R.J. Krane, The likely worldwide increase in erectile dysfunction between 1995 and 2025 and some possible policy consequences, BJU Int. 84 (1) (1999) 50–56.
[2] H.A. Feldman, I. Goldstein, D.G. Hatzichristou, R.J. Krane, J.B. McKinlay, Impotence and its medical and psychosocial correlates: results of the Massachusetts Male Aging Study, J. Urol. 151 (1) (1994) 54–61.
[3] M.G. Ferrini, N.F. Gonzalez-Cadavid, J. Rajfer, Aging related erectile dysfunction—potential mechanism to halt or delay its onset, Transl. Androl. Urol. 6 (1) (2017) 20.
[4] E.A. Jannini, S. Droupy, Needs and expectations of patients with erectile dysfunction: an update on pharmacological innovations in phosphodiesterase type 5 inhibition with focus on sildenafil, Sex. Med. 7 (1) (2019) 1–10.
[5] A. Salonia, et al., European association of urology guidelines on sexual and reproductive health—2021 update: male sexual dysfunction, Eur. Urol. 80 (3) (2021) 333–357.
[6] P. Bajic, J. Mahon, M. Faraday, H. Sadeghi-Nejad, L. Hakim, K.T. McVary, Etiology of erectile dysfunction and duration of symptoms in patients undergoing penile prosthesis: a systematic review, Sex. Med. Rev. 8 (2) (2020) 333–337.
[7] D.J. Lee, et al., Trends in the utilization of penile prostheses in the treatment of erectile dysfunction in the United States, J. Sex. Med. 12 (7) (2015) 1638–1645.
[8] H.L. Chou, N.A. Mohsen, B.B. Garber, D.C. Feldstein, CT imaging of inflatable penile prosthesis complications: a pictorial essay, Abdom. Radiol. 44 (2) (2019) 739–748.
[9] L. Trost, W.J. Hellstrom, History, contemporary outcomes, and future of penile prostheses: a review of the literature, Sex. Med. Rev. 1 (3) (2013) 150–163.
[10] D. Udelson, et al., Engineering analysis of penile hemodynamic and structural-dynamic relationships: Part I—clinical implications of penile tissue mechanical properties, Int. J. Impot. Res. 10 (1) (1998) 15–24.
[11] D. Udelson, et al., Engineering analysis of penile hemodynamic and structural-dynamic relationships: Part II—clinical implications of penile buckling, Int. J. Impot. Res. 10 (1) (1998) 25–35.
[12] J. Chen, A. Gefen, A. Greenstein, H. Matzkin, D. Elad, Predicting penile size during erection, Int. J. Impot. Res. 12 (6) (2000) 328–333.
[13] A. Gefen, J. Chen, D. Elad, Optimization of design and surgical positioning of inflatable penile prostheses, Ann. Biomed. Eng. 28 (6) (2000) 619–628.
[14] A. Gefen, J. Chen, D. Elad, Stresses in the normal and diabetic human penis following implantation of an inflatable prosthesis, Med. Biol. Eng. Comput. 37 (5) (1999) 625–631.
[15] A.M. Mohamed, A.G. Erdman, G.W. Timm, The biomechanics of erections: two- versus one-compartment pressurized vessel modeling of the penis, J. Biomech. Eng. 132 (12) (2010) 121004–121012.
[16] E.R.A.N. Linder-Ganz, A. Gefen, D. Elad, J. Chen, A three-dimensional model of the penis for analysis of tissue stresses during normal and abnormal Erection, Ann. N. Y. Acad. Sci. 1101 (1) (2007) 464–476.
[17] G.W. Timm, et al., Tissue characterization for improved external penile occlusive device design, Trans. ASME (Am. Soc. Mech. Eng.) J. Biomech. Eng. 127 (2005) 956–963.
[18] A. Levy, M. Fader, D. Bader, A. Gefen, Penile compression clamps: a model of the internal mechanical state of penile soft tissues, Neurourol. Urodyn. 36 (6) (2017) 1645–1650.
[19] M. Bitsch, B. Kromann-Andersen, J. Schou, E. Sjøntoft, The elasticity and the tensile strength of tunica albuginea of the corpora cavernosa, J. Urol. 143 (3) (1990) 642–645.
[20] L. Brady, et al., Mechanical characterization of fibrotic and mineralized tissue in Peyronie's disease, Int. J. Impot. Res. 34 (5) (2021) 477–486.
[21] E. Inci, R. Turkay, M.O. Nalbant, M.G. Yenice, V. Tugcu, The value of shear wave elastography in the quantification of corpus cavernosum penis rigidity and its alteration with age, Eur. J. Radiol. 89 (2017) 106–110.
[22] X. Zhang, B. Zhou, S.L. Kopecky, L.W. Trost, Two dimensional penile ultrasound vibro-elastography for measuring penile tissue viscoelasticity: a pilot patient study and its correlation with penile ultrasonography, J. Mech. Behav. Biomed. Mater. 103 (2020), 103570.
[23] J.J. Zhang, et al., A new method of measuring the stiffness of corpus cavernosum penis with ShearWaveTM Elastography, Br. J. Radiol. 88 (1048) (2015), 20140671.
[24] V. Purpura, et al., The development of a decellularized extracellular matrix–based biomaterial scaffold derived from human foreskin for the purpose of foreskin reconstruction in circumcised males, J. Tissue Eng. 9 (2018), 2041731418812613.
[25] S. Bose, B. Fereidoonnezhad, M. Akbarzadeh Khorshidi, B. Watschke, E. Mareena, D. Nolan, S. Cooney, I.M. Cullen, C. Lally, The role of tissue biomechanics in the implantation and performance of inflatable penile prostheses: current state of the art and future perspective, Sexual Medicine Reviews 1–10 (2023) qead013.
[26] L. Rouleau, D. Tremblay, R. Cartier, R. Mongrain, R.L. Leask, Regional variations in canine descending aortic tissue mechanical properties change with formalin fixation, Cardiovasc. Pathol. 21 (5) (2012) 390–397.
[27] A. Kirkham, MRI of the penis, Br. J. Radiol. 85 (1) (2012) S86–S93.
[28] J.S. Bergstrom, Mechanics of Solid Polymers: Theory and Computational Modeling, William Andrew, 2015.
[30] D.A. Kelly, Expansion of the tunica albuginea during penile inflation in the nine-banded armadillo (Dasypus novemcinctus), J. Exp. Biol. 202 (3) (1999) 253–265.
[31] G.-L. Hsu, G. Brock, L. Martinez-Pineiro, B. Von Heyden, T.F. Lue, E.A. Tanagho, Anatomy and strength of the tunica albuginea: its relevance to penile prosthesis extrusion, J. Urol. 151 (1994) 1205–1208.
[32] G.-L. Hsu, G. Brock, B. Von Heyden, L. Nunes, T.F. Lue, E.A. Tanagho, The distribution of elastic fibrous elements within the human penis, Br. J. Urol. 73 (1994) 566–571.
[33] D.A. Kelly, Axial orthogonal fiber reinforcement in the corpus cavernosum of the nine banded armadillo (Dasypus novemcinctus), J. Morphol. 233 (1997) 249–255.
[34] G.A. Holzapfel, T.C. Gasser, R.W. Ogden, A new constitutive framework for arterial wall mechanics and a comparative study of material models, J. Elasticity 61 (2000) 1–48.
[35] T.C. Gasser, R.W. Ogden, G.A. Holzapfel, Hyperelastic modelling of arterial layers with distributed collagen fibre orientations, J. R. Soc. Interface 3 (6) (2006) 15–35.